Electronic Supplementary Information (ESI) †

Nanomat Li-S batteries based on all-fibrous cathode/separator assemblies and reinforced Li metal anodes: Towards ultrahigh energy density and flexibility

Jung-Hwan Kim,[a] Yong-Hyeok Lee,[a] Sung-Ju Cho,[a] Jae-Gyoung Gwon,[b] Hye-Jung Cho,[b] Minchul Jang,[c] Sun-Young Lee,[b,*] and Sang-Young Lee[a,*]

[a]Department of Energy Engineering, School of Energy and Chemical Engineering, Ulsan National Institute of Science and Technology (UNIST), Ulsan, 44919, Republic of Korea. *E-mail: syleek@unist.ac.kr

[b]Department of Forest Products, National Institute of Forest Science, Seoul, 02455, Republic of Korea. *E-mail: nararawood@korea.kr

[c]Future Technology Research Center, LG Chem., Seoul, 07796, Republic of Korea.

Table S1. Summary of the major component specifications and volumetric cell capacities: nanomat Li-S cell vs. previously reported flexible Li-S cells.[SR1-24] Note that some of the previous works did not reveal the thicknesses of lithium metal electrodes and current collectors. Here, to provide a quantitative comparison, these values were assumed to be 120 (lithium metal electrodes) and 20 μm (current collectors), respectively, from the product information (the thinnest ones practically available) of Sigma-Aldrich.

Ref.	Characteristic	Areal mass loading of sulfur	Areal capacity	Electrode thickness	Separator thickness	Li metal thickness	Current collector thickness	Cell thickness	Sulfur loading (per cell volume)	Volumetric cell capacity
		mg cm^{-2}	mAh cm^{-2}	μm	μm	μm	μm	μm	g mL_{cell}^{-1}	Ah L_{cell}^{-1}
This work	Nanomat Li-S cell (Cathode-separator assembly + Reinforced Li metal)	3.10	2.7	50	-	55	-	105	0.29	257.14
		6.36	5.16	95	-	55	-	150	0.42	344
		9.28	7.54	135	-	55	-	190	0.46	396.84
SR1	MOF@CNT@S	4.57	3.59	30.4	25	120	20	195.4	0.23	183.72
SR2	rGO@PEDOT:PSS@S	3	3.3	30.3	25	120	20	195.3	0.15	168.97
SR3	Li_2S@NCNF	3	2.2	150	25	120	20	315	0.09	69.84
SR4	SWNT/CNF+CNF/S	4	3.8	100	25	120	20	265	0.15	143.39
SR5	CF@CNTs/MgO-S	3.8	3.65	5000	25	120	20	5165	0.01	7.066
SR6	NG@S-CNT	4.7	3.96	70	25	1000	20	1115	0.042	35.51
SR7	S/G/NPCFs	1.1	0.89	50	25	120	20	215	0.051	41.39
SR8	3D graphene sponges composite	2	0.84	100	25	120	20	265	0.075	31.69
SR9	N-doped carbon foam	1.2	1	2500	25	120	20	2665	0.004	3.75
SR10	CNT/ACNF@MnO2-S	2.4	2.01	70	25	120	20	235	0.1	85.53
SR11	CNT/S/CNT	3.2	2.26	100	25	120	20	265	0.12	85.28
SR12	NCPT+MWNT/S	3	2.55	150	25	120	20	315	0.095	80.95
SR13	C/S/C	0.83	0.91	50	25	120	20	215	0.038	42.32
SR14	GF-rGO/S	9.8	6.86	1400	25	120	20	1565	0.062	43.83
SR15	S-rGO paper	1	0.97	50	25	120	20	215	0.046	45.11
SR16	CNT current collector	6.8	4.8	80	25	120	6	231	0.29	207.79
SR17	S-G@PP	2.1	1.78	70	25	120	20	235	0.089	75.74
SR18	G-NDHCS-S	3.9	3.86	120	25	120	20	285	0.13	135.43
SR19	S-CP@TiO_2	2	2.2	90	25	120	-	235	0.085	93.61
SR20	VACNT-MWCNT@S	6.3	5	250	25	120	20	415	0.15	120.48
SR21	S/CNT/C	2.3	1.9	50	25	120	20	215	0.1	88.37
SR22	S-CNT	3	2.6	40	25	120	20	205	0.14	126.82
SR23	GS/S	1.53	0.95	50	25	120	20	215	0.07	44.18
SR24	S-CNT	1.25	0.71	70	25	120	-	215	0.058	33.02

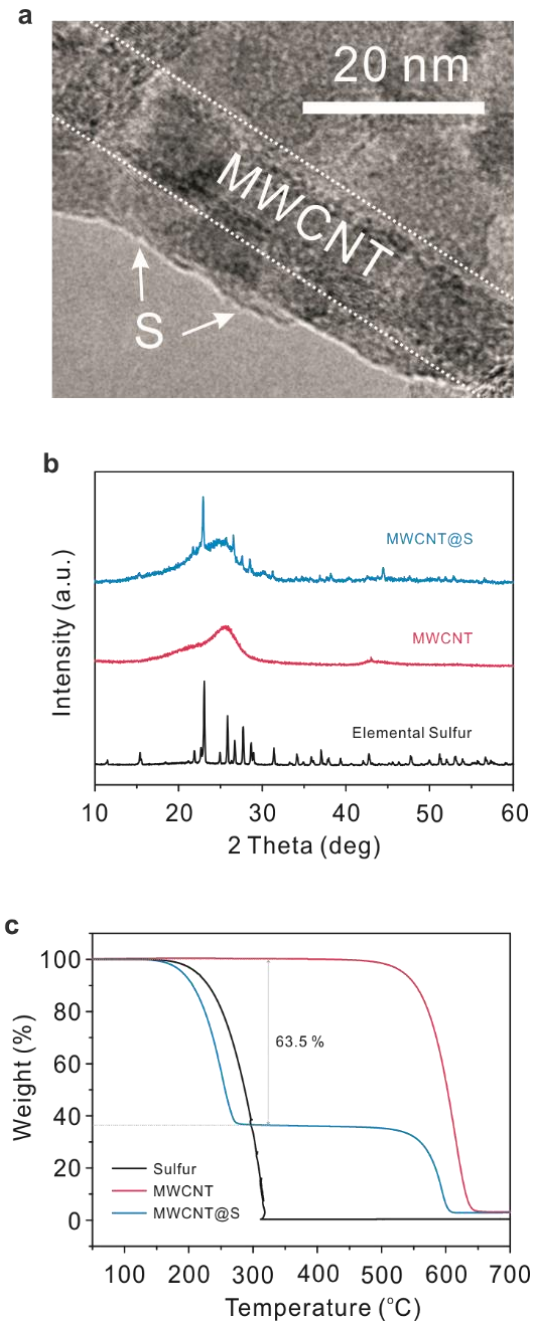

Fig. S1. Structural characteristics of MWCNT@S. (a) TEM image. (b) XRD patterns. (c) TGA profiles.

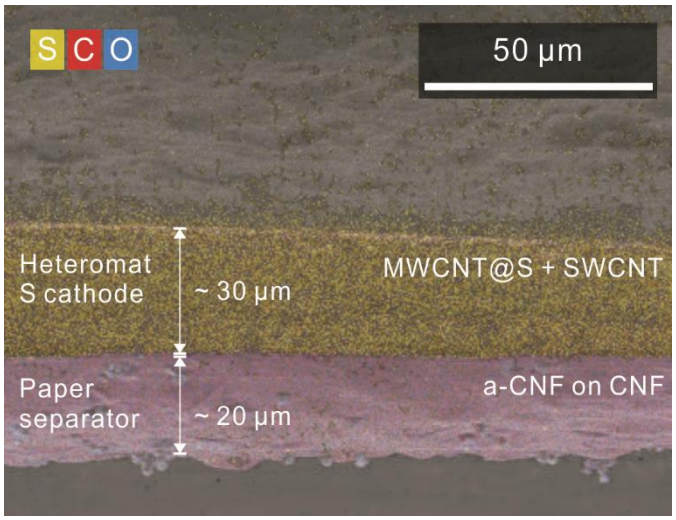

Fig. S2. SEM image (cross-sectional) of a cathode-separator assembly showing the seamless integration of the heteromat-structured sulfur cathode (~ 30 µm) and bi-layered paper separator (~ 20 µm).

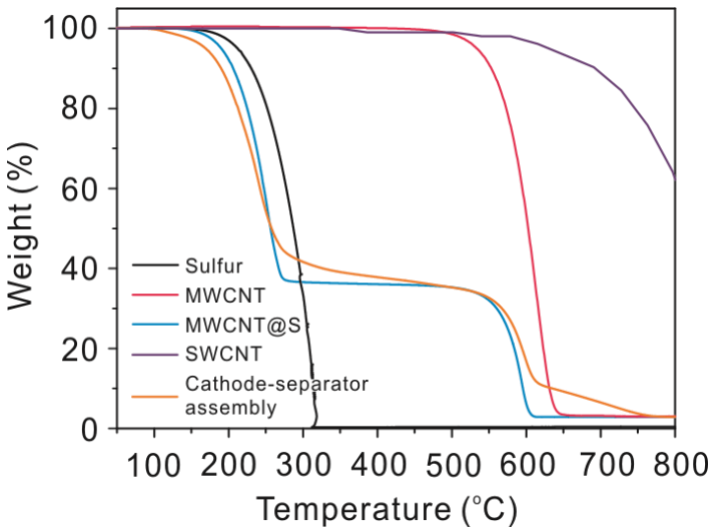

Fig. S3. TGA profiles of the cathode-separator assembly. The results of the major components themselves are also provided for comparison.

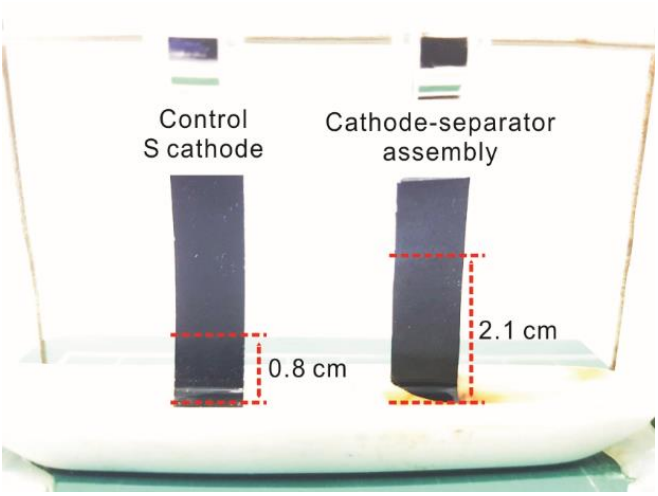

Fig. S4. Comparison of the electrolyte immersion height: control sulfur cathode vs. cathode-separator assembly.

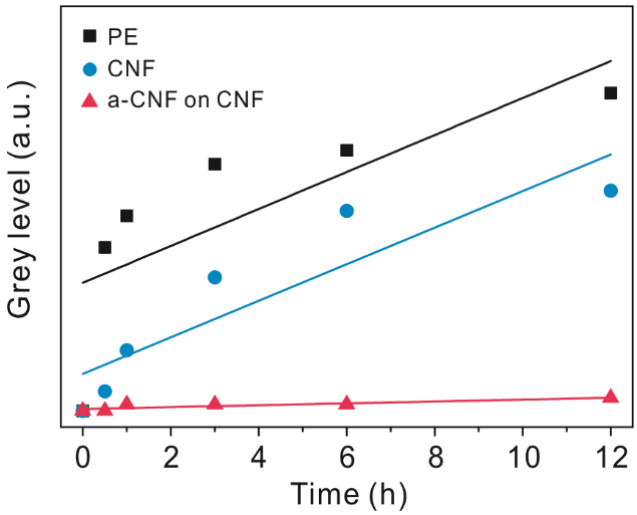

Fig. S5. Change in the grey level in the bottom of the tubes (shown in Fig. 2h) as a function of elapsed time.

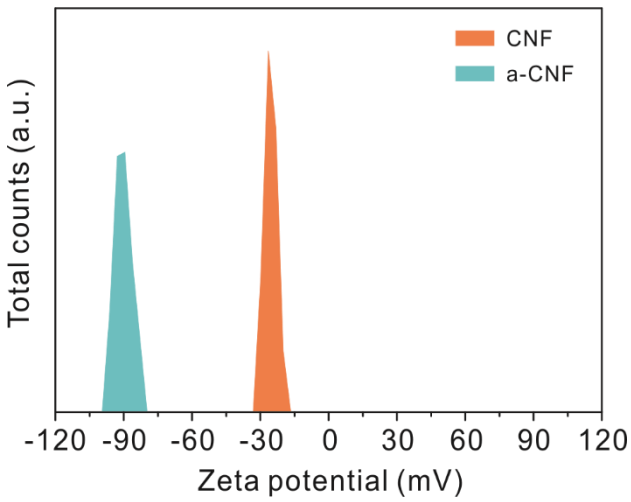

Fig. S6. Zeta potential of the pristine CNFs and a-CNFs.

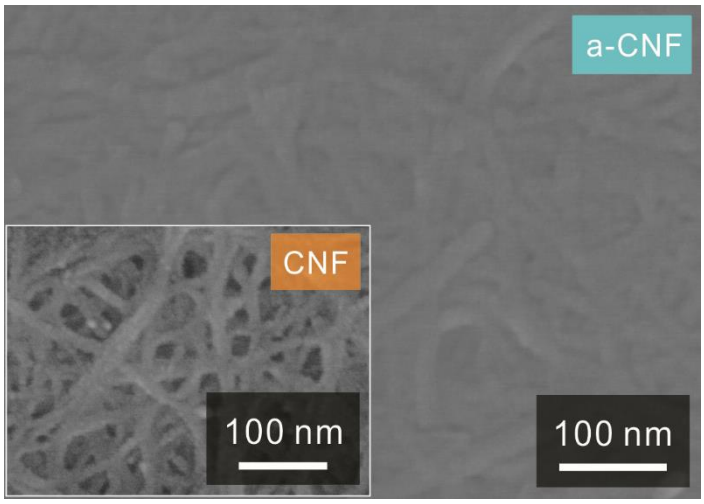

Fig. S7. SEM images of the a-CNF layer and pristine CNF layer (inset).

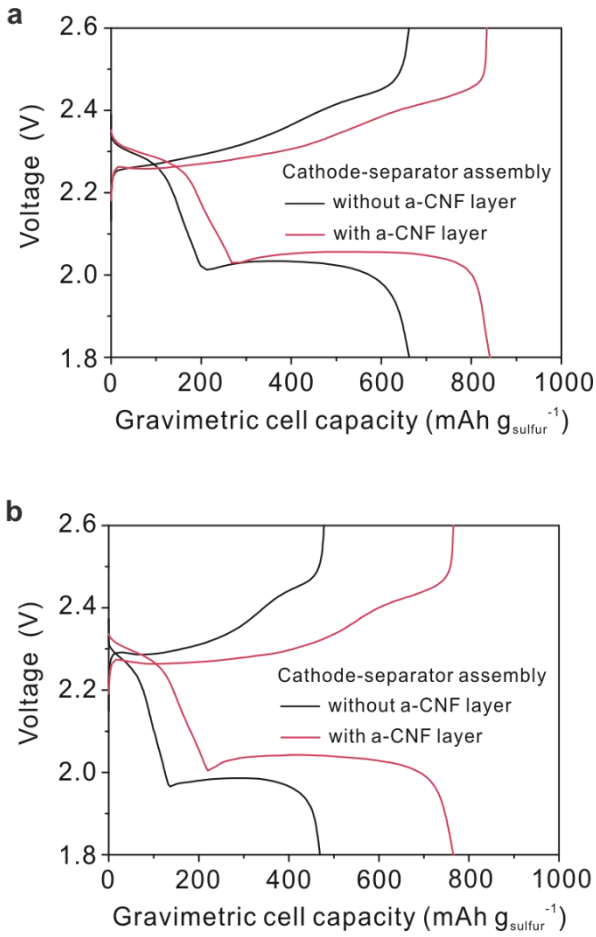

Fig. S8. Galvanostatic charge/discharge profiles of Li-S cells assembled with different cathode-separator assemblies (a-CNF layer vs. CNF layer) at a charge/discharge current density of 1.0 C/1.0 C. (a) 1st cycle. (b) 200th cycle.

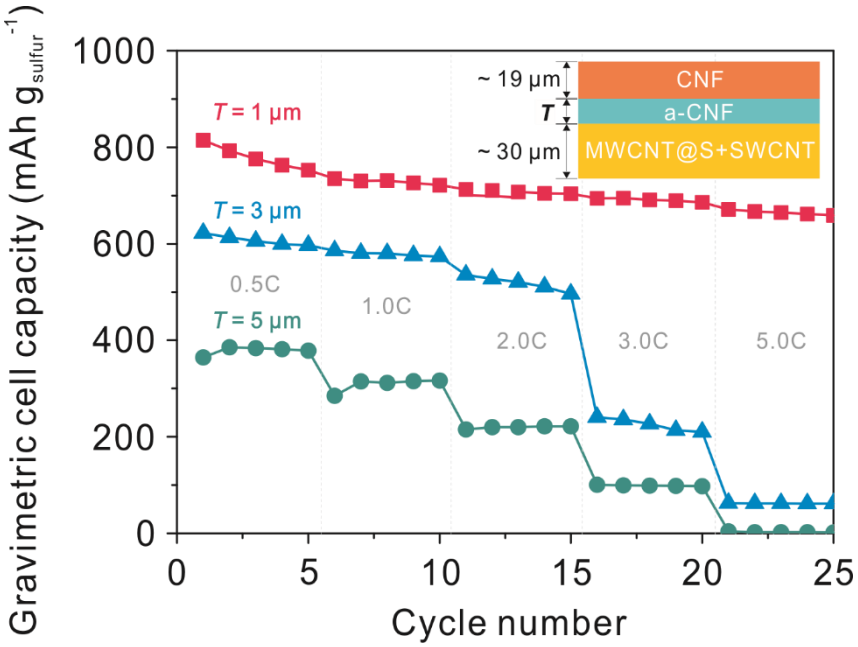

Fig. S9. Comparison of the discharge rate capabilities of the cathode-separator assemblies as a function of a-CNF layer thickness, in which the cells were discharged at various current densities (0.2 - 5.0 C) under a fixed charge current density of 0.5 C between 1.8 to 2.6 V.

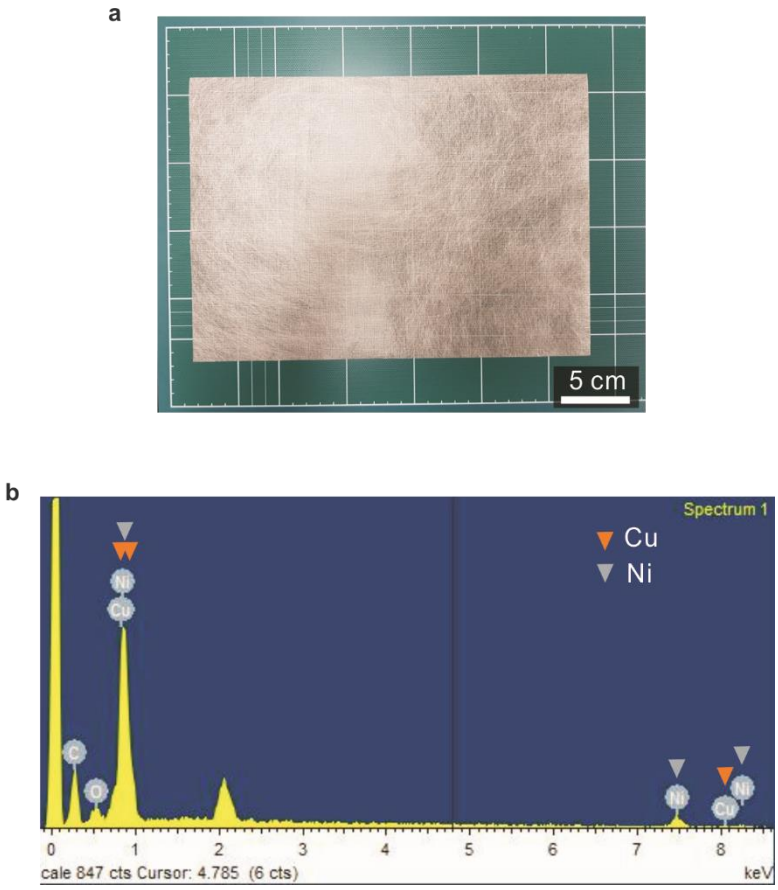

Fig. S10. (a) Photograph of the (Ni/Cu-plated) conductive PET nonwoven. (b) EDS profile.

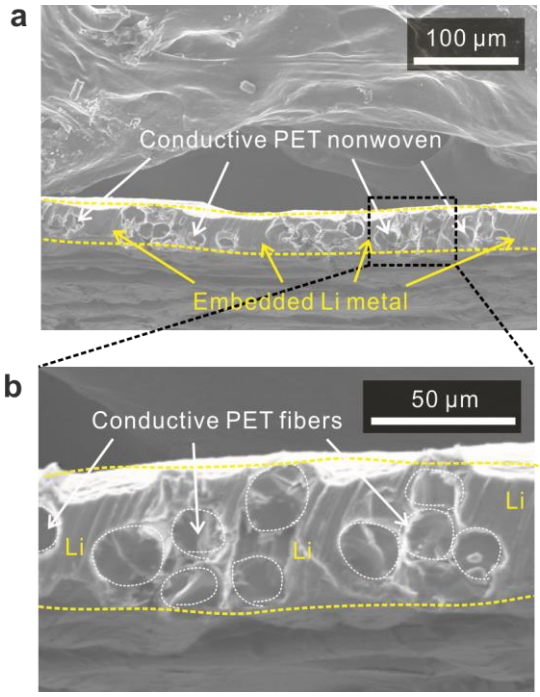

Fig. S11. Cross-sectional SEM images of the reinforced Li metal. (a) Low magnification. (b) High magnification.

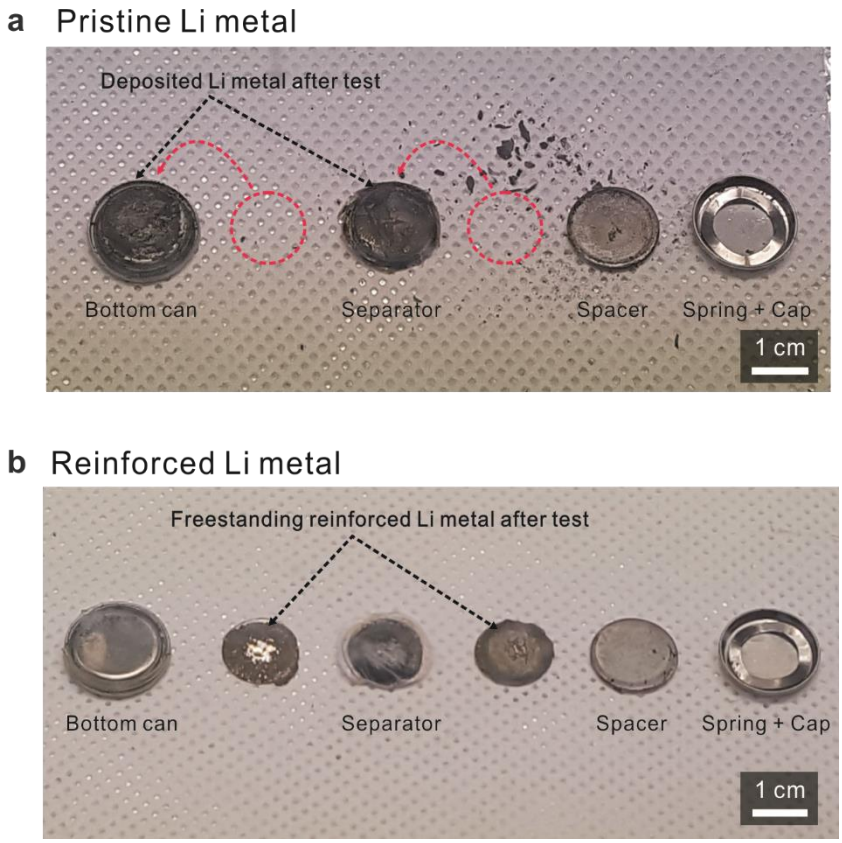

Fig. S12. Photographs of the disassembled cell components after the repeated plating/stripping test. (a) Pristine Li metal electrode. (b) Reinforced Li metal electrode.

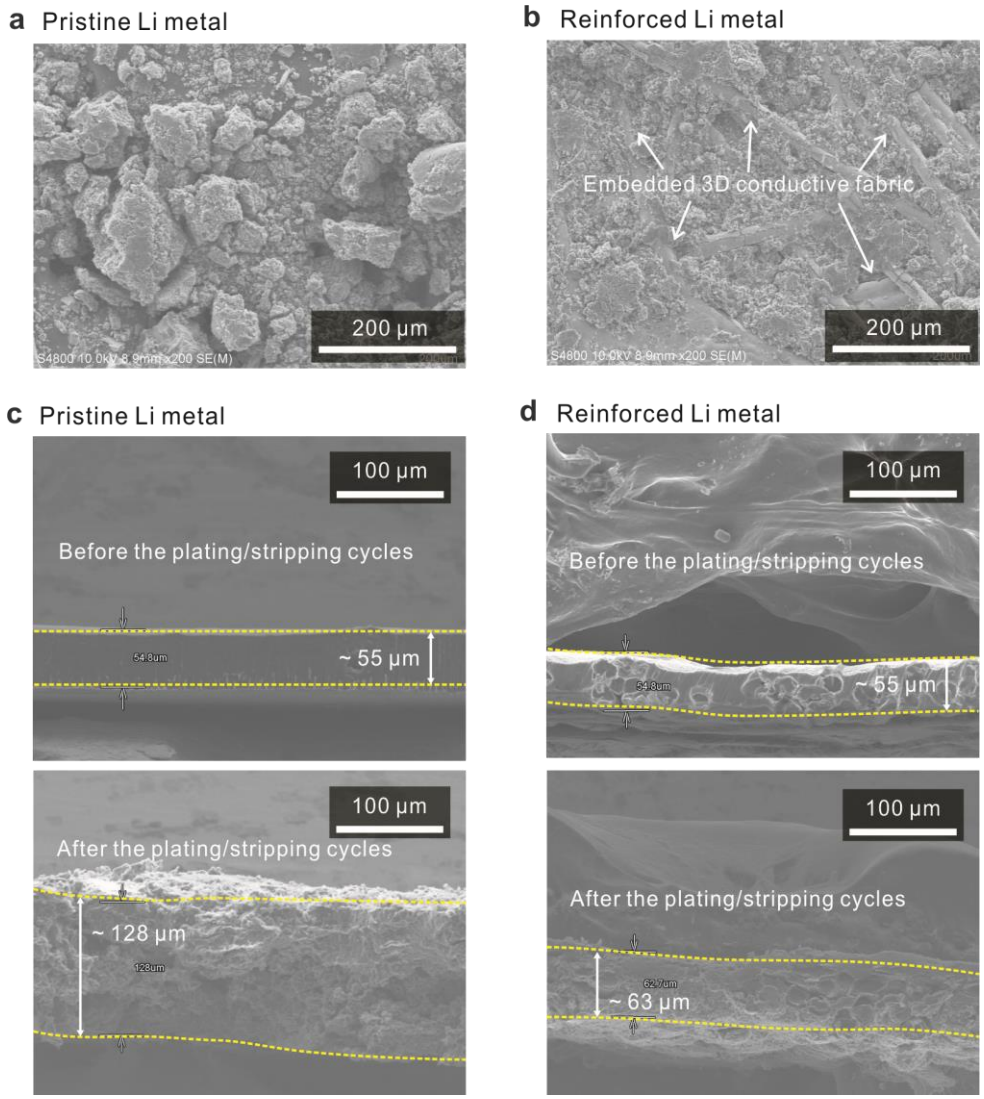

Fig. S13. Comparison of SEM images (pristine Li metal electrode vs. reinforced Li metal electrode). (a) and (b) Surface view. (c) and (d) Cross-sectional view (before and after the plating/stripping cycles).

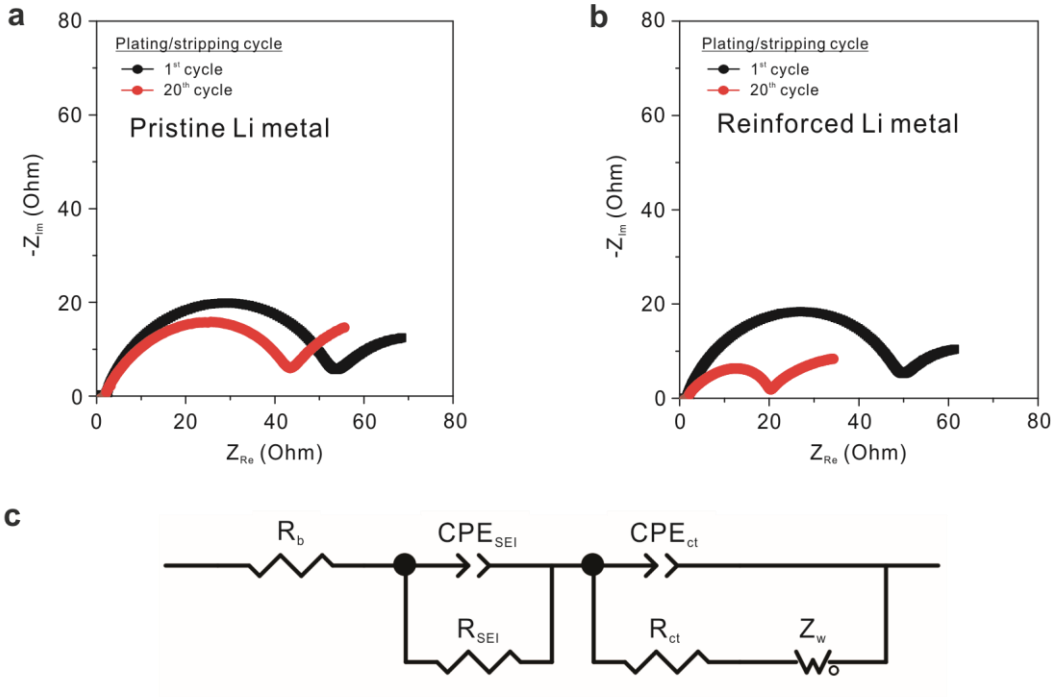

Sample	After 1st cycle			After 20th cycle		
	R_b	R_{SEI}	R_{ct}	R_b	R_{SEI}	R_{ct}
Pristine Li metal	1.89	5.21	41.9	1.99	6.17	35.9
Reinforced Li metal	1.82	5.42	37.5	1.79	3.51	13.4

* Unit of R_b, R_{SEI} and R_{ct}: ohm.
* R_b is bulk resistance, R_{SEI} is the solid electrolyte interface resistance, R_{ct} is the charge transfer resistance.
* CPE_{SEI} and CPE_{ct} are the constant phase element at high and low frequencies, respectively.

Fig. S14. Electrochemical impedance spectroscopy (EIS) profiles (at the 1st and 20th cycle) of (a) the pristine Li metal and (b) reinforced Li metal electrodes. (c) Equivalent circuit diagram for the EIS plots and summary of the fitted parameters.

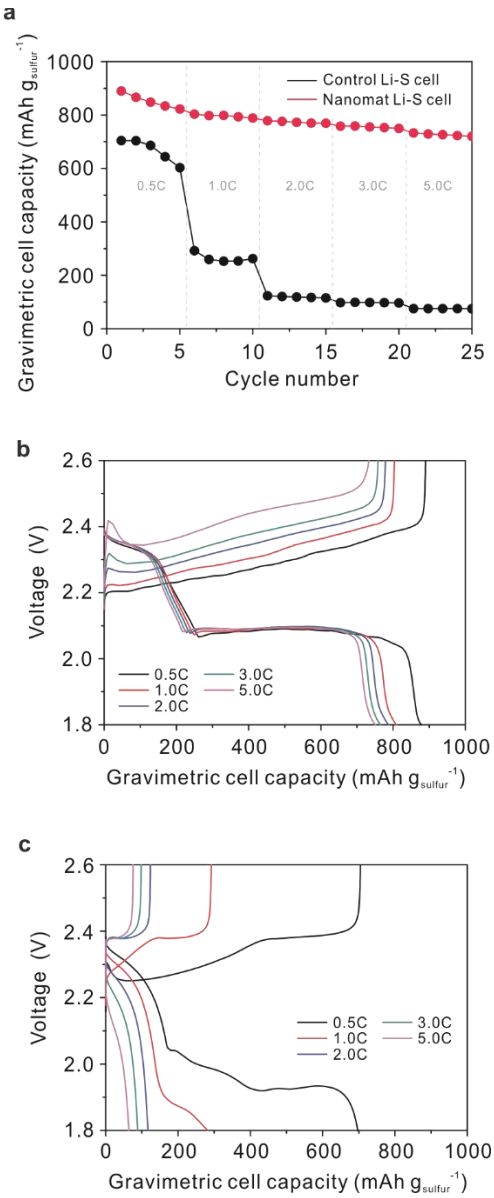

Fig. S15. (a) Comparison of the discharge rate capability between nanomat and control Li-S cells. Discharge profiles of (b) the nanomat Li-S cell and (c) control Li-S cell. The gravimetric discharge capacities of the cells were expressed based on the sulfur mass loading (mAh g_{sulfur}^{-1}). The discharge current densities varied from 0.2 to 5.0 C at a fixed charge current density of 0.2 C under a voltage range of 1.8 − 2.6 V.

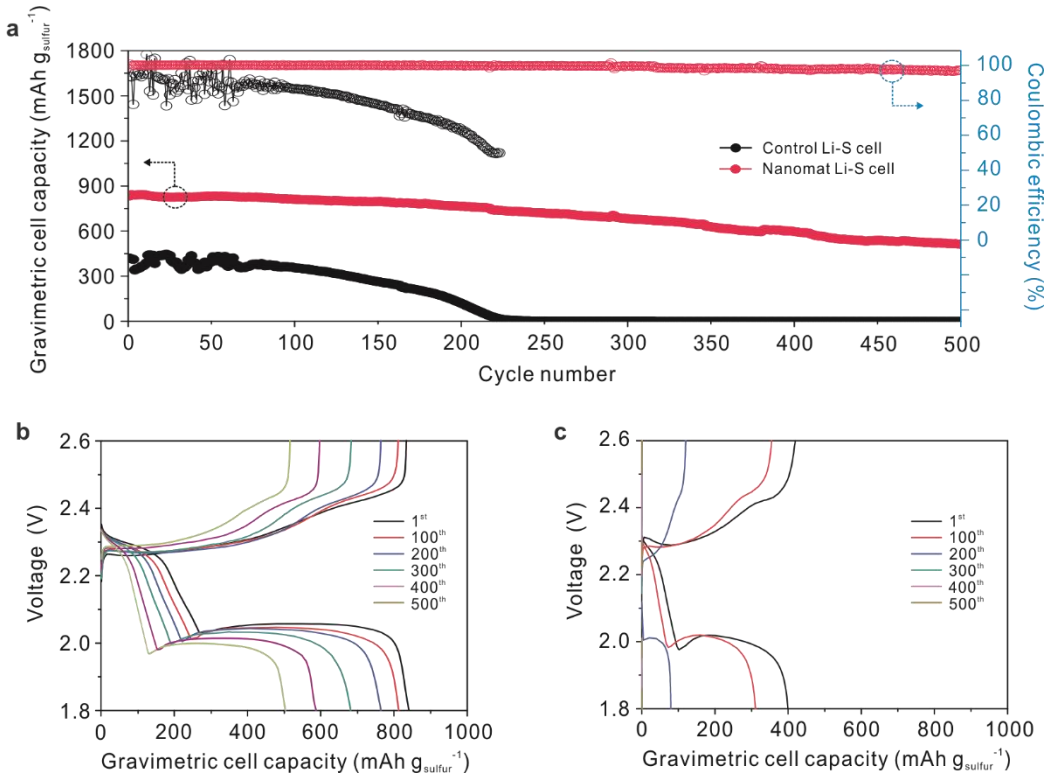

Fig. S16. (a) Cycling performance (charge/discharge current density = 1.0 C/1.0 C) of the nanomat and control Li-S cells. Galvanostatic charge/discharge profiles of (b) the nanomat Li-S cell and (c) control Li-S cell. The charge/discharge capacities of the cells were expressed based on the sulfur mass loading (mAh g_{sulfur}^{-1}).

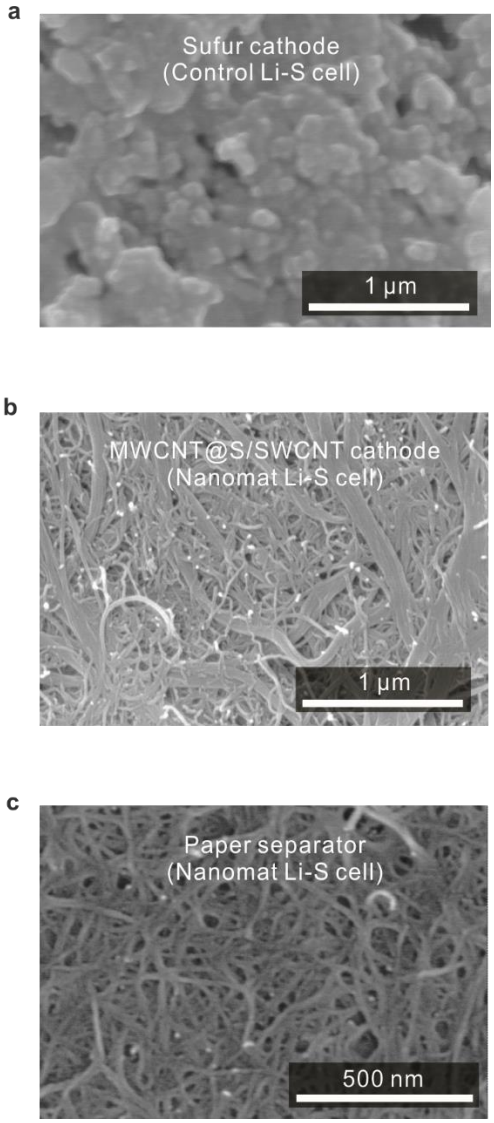

Fig. S17. SEM images of the nanomat and control Li-S cells after the cycling test (500 cycles). (a) Control sulfur cathode. (b) Heteromat (MWCNT@S/SWCNT) sulfur cathode. (c) Paper separator.

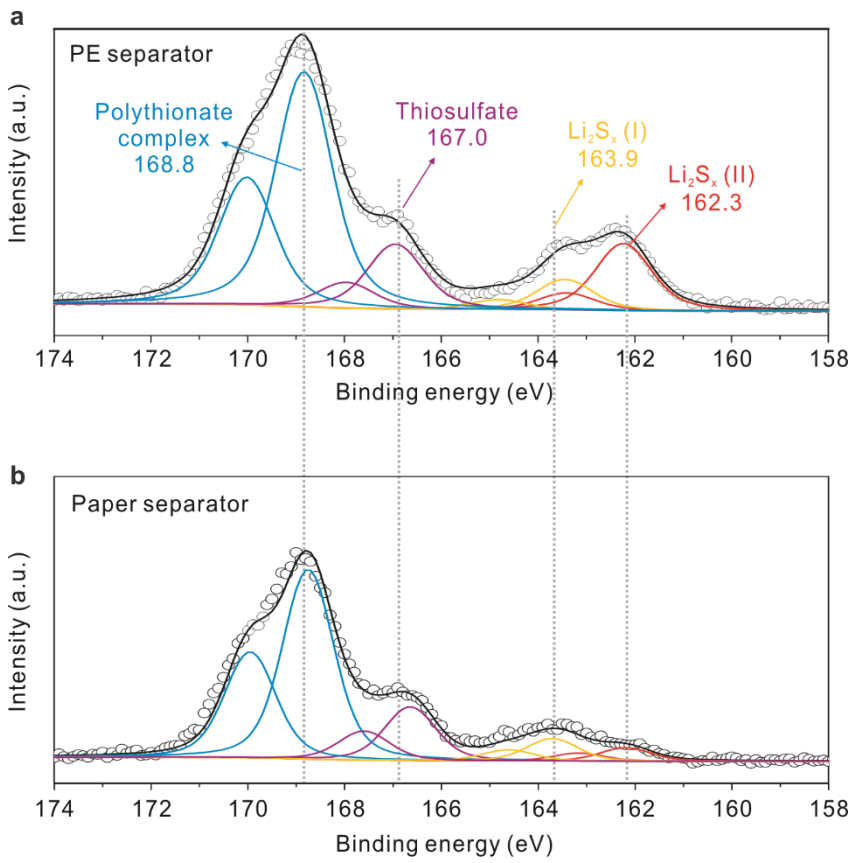

Fig. S18. XPS profiles of the PE and paper separators (facing the Li metal anodes) after the cycling test (500 cycles).

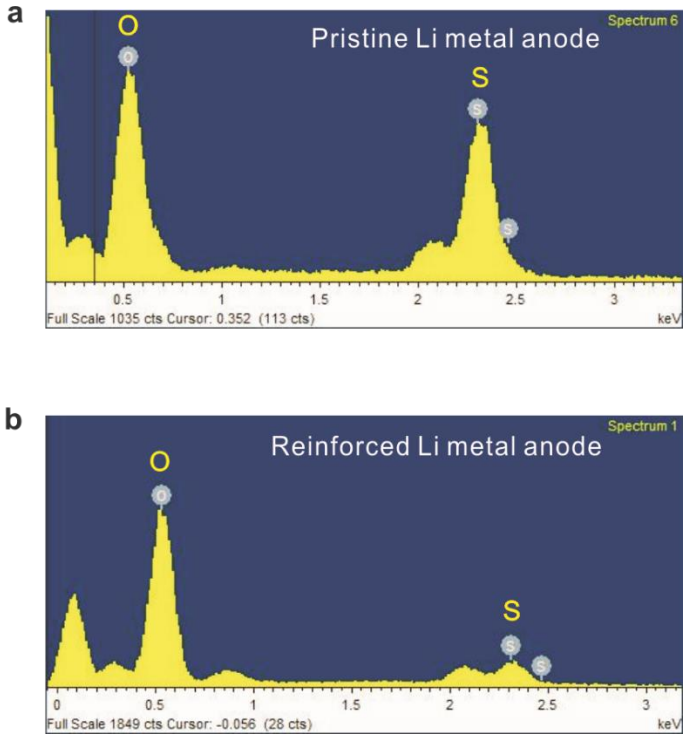

Fig. S19. EDS profiles (focusing on the sulfur element) after the cycling test (500 cycles). (a) Pristine Li metal anode. (b) Reinforced Li metal anode.

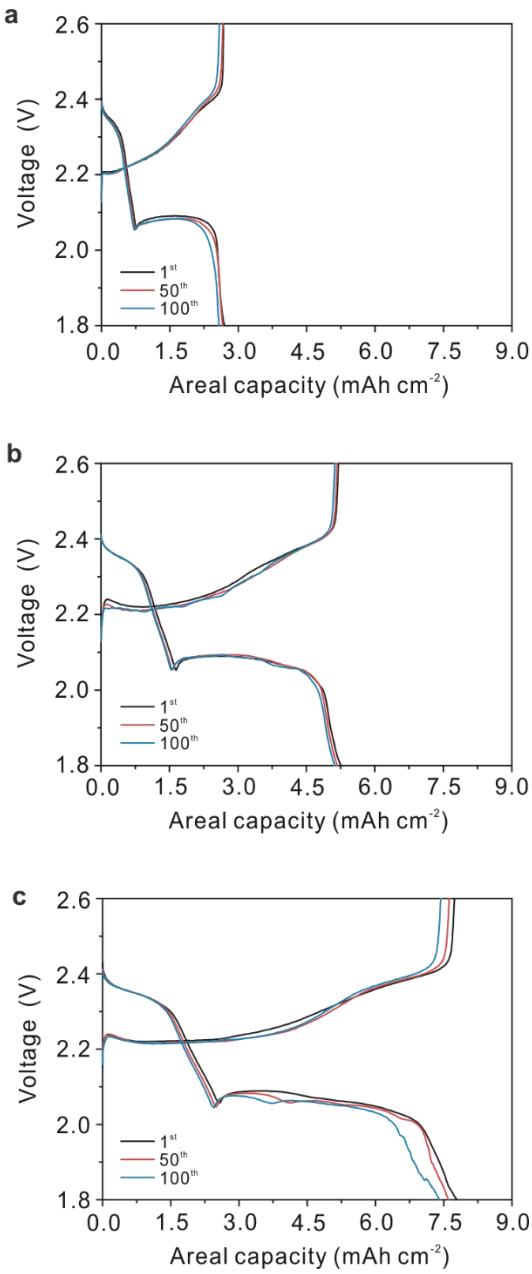

Fig. S20. Galvanostatic charge/discharge profiles (voltage vs. areal capacities, measured at a charge/discharge current density of 0.2 C/0.2 C) of the nanomat Li-S cells fabricated with different cathode-separator assemblies as a function of sulfur mass loading. (a) Areal mass loading of sulfur = 3.10 mg cm^{-2}. (b) 6.36 mg cm^{-2}. (c) 9.28 mg cm^{-2}.

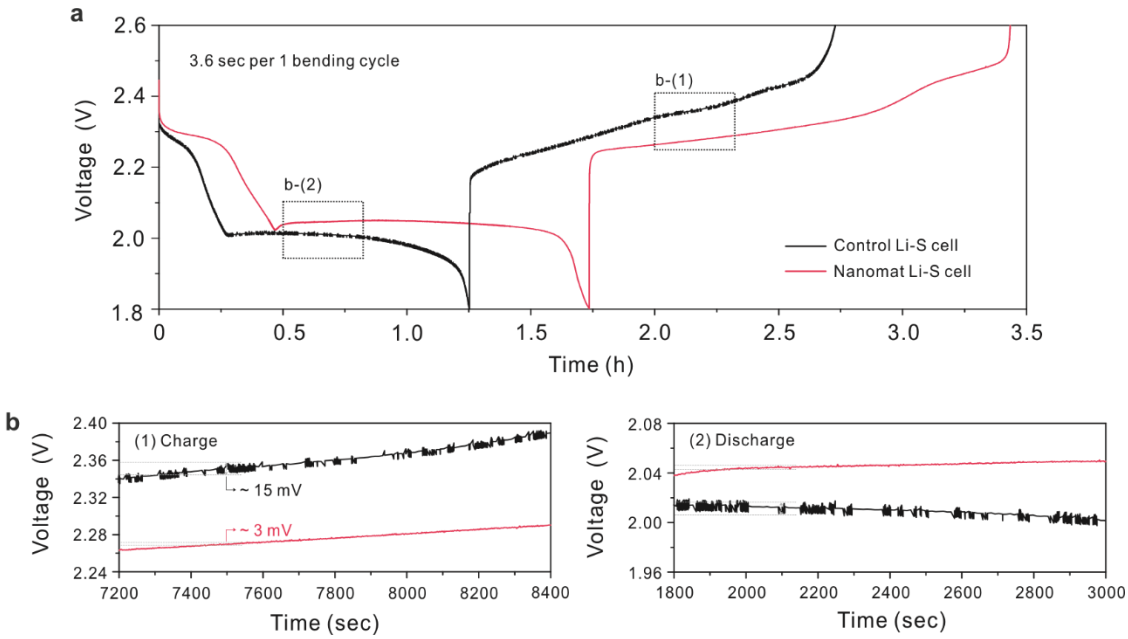

Fig. S21. (a) *In situ* monitoring of the cell voltage during charge/discharge reaction upon repeated bending deformation (bending radius = 2.5 mm and deformation rate = 500 mm min^{-1}). (b) High-magnification view of the charge/discharge profiles.

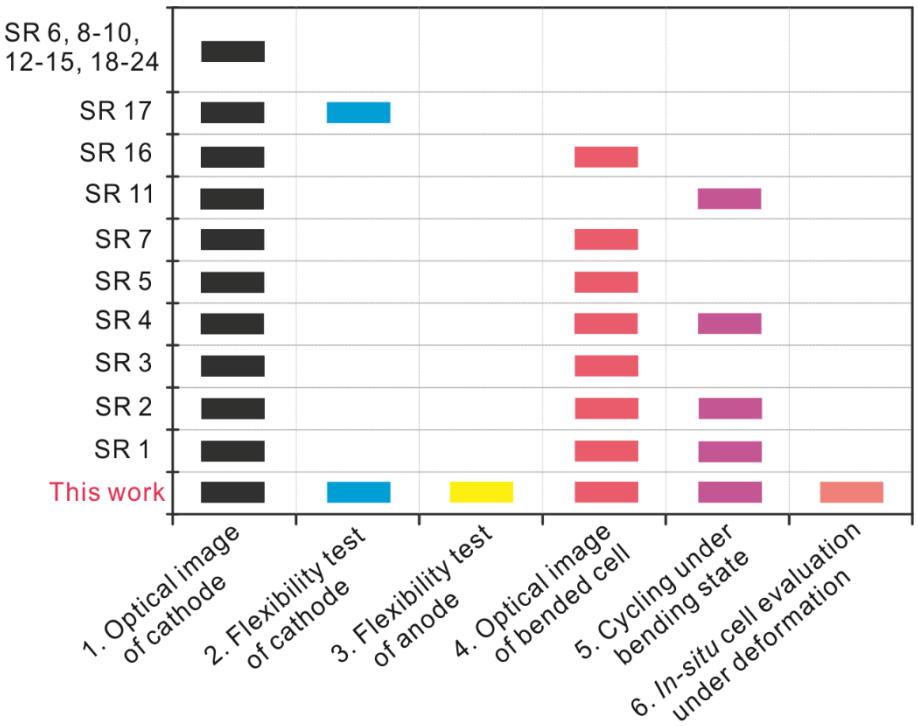

Fig. S22. Summary of the analysis modes used to elucidate the mechanical deformability: nanomat Li-S cell vs. previously reported flexible Li-S cells (Supplementary references SR1-24).

Supplementary References

SR1 Y. Mao, G. Li, Y. Guo, Z. Li, C. Liang, X. Peng and Z. Lin, *Nat. Commun.*, 2017, **8**, 14628.

SR2 P. Xiao, F. Bu, G. Yang, Y. Zhang and Y. Xu, *Adv. Mater.*, 2017, **29**, 1703324.

SR3 M. Yu, Z. Wang, Y. Wang, Y. Dong and J. Qiu, *Adv. Energy Mater.*, 2017, **7**, 1700018.

SR4 C.-H. Chang, S.-H. Chung and A. Manthiram, *Mater. Horiz.*, 2017, **4**, 249-258.

SR5 M. Xiang, H. Wu, H. Liu, J. Huang, Y. Zheng, L. Yang, P. Jing, Y. Zhang, S. Dou and H. Liu, *Adv. Funct. Mater.*, 2017, **27**, 1702573.

SR6 P.-Y. Zhai, J.-Q. Huang, L. Zhu, J.-L. Shi, W. Zhu and Q. Zhang, *Carbon*, 2017, **111**, 493-501.

SR7 X. Song, S. Wang, Y. Bao, G. Liu, W. Sun, L.-X. Ding, H. Liu and H. Wang, *J. Mater. Chem. A*, 2017, **5**, 6832-6839.

SR8 C. Lin, C. Niu, X. Xu, K. Li, Z. Cai, Y. Zhang, X. Wang, L. Qu, Y. Xu and L. Mai, *Phys. Chem. Chem. Phys.*, 2016, **18**, 22146-22153.

SR9 Z. Cao, J. Zhang, Y. Ding, Y. Li, M. Shi, H. Yue, Y. Qiao, Y. Yin and S. Yang, *J. Mater. Chem. A*, 2016, **4**, 8636-8644.

SR10 H. Xu, L. Qie and A. Manthiram, *Nano Energy*, 2016, **26**, 224-232.

SR11 S. H. Chung, C. H. Chang and A. Manthiram, *Small*, 2016, **12**, 939-950.

SR12 H. S. Kang and Y. K. Sun, *Adv. Funct. Mater.*, 2016, **26**, 1225-1232.

SR13 H. Wang, W. Zhang, H. Liu and Z. Guo, *Angew. Chem. Int. Ed.*, 2016, **55**, 3992-3996.

SR14 G. Hu, C. Xu, Z. Sun, S. Wang, H. M. Cheng, F. Li and W. Ren, *Adv. Mater.*, 2016, **28**, 1603-1609.

SR15 C. Wang, X. Wang, Y. Wang, J. Chen, H. Zhou and Y. Huang, *Nano Energy*, 2015, **11**, 678-686.

SR16 L. Li, Z. P. Wu, H. Sun, D. Chen, J. Gao, S. Suresh, P. Chow, C. V. Singh and N. Koratkar, *ACS Nano*, 2015, **9**, 11342-11350.

SR17 G. Zhou, L. Li, D. W. Wang, X. y. Shan, S. Pei, F. Li and H. M. Cheng, *Adv. Mater.*, 2015, **27**, 641-647.

SR18 G. Zhou, Y. Zhao and A. Manthiram, *Adv. Energy Mater.*, 2015, **5**, 1402263.

SR19 Z. Zhang, Q. Li, K. Zhang, W. Chen, Y. Lai and J. Li, *J. Power Sources*, 2015, **290**, 159-167.

SR20 Z. Yuan, H. J. Peng, J. Q. Huang, X. Y. Liu, D. W. Wang, X. B. Cheng and Q. Zhang, *Adv. Funct. Mater.*, 2014, **24**, 6105-6112.

SR21 J.-Q. Huang, H.-J. Peng, X.-Y. Liu, J.-Q. Nie, X.-B. Cheng, Q. Zhang and F. Wei, *J. Mater. Chem. A*, 2014, **2**, 10869-10875.

SR22 K. Jin, X. Zhou, L. Zhang, X. Xin, G. Wang and Z. Liu, *J. Phys. Chem. C*, 2013, **117**, 21112-21119.

SR23 J. Jin, Z. Wen, G. Ma, Y. Lu, Y. Cui, M. Wu, X. Liang and X. Wu, *RSC Adv.*, 2013, **3**, 2558-2560.

SR24 G. Zhou, D.-W. Wang, F. Li, P.-X. Hou, L. Yin, C. Liu, G. Q. M. Lu, I. R. Gentle and H.-M. Cheng, *Energy Environ. Sci.*, 2012, **5**, 8901-8906.